

# Effect of Ca doping on the performance of CeO<sub>2</sub>–NiO catalysts for CH<sub>4</sub> catalytic combustion

Dongsheng Qiao · Guanzhong Lu · Dongsen Mao ·  
Yun Guo · Yanglong Guo

Received: 7 March 2010 / Accepted: 21 July 2010 / Published online: 10 August 2010  
© Springer Science+Business Media, LLC 2010

**Abstract** Methane catalytic combustion was carried out over the Ce<sub>0.9-x</sub>Ni<sub>0.1</sub>Ca<sub>x</sub>O<sub>δ</sub> (0 < x ≤ 0.3) catalysts prepared by a citric acid complexation–combustion method. When x ≤ 0.1, the presence of Ca can enhance the surface area and reduce the crystalline size, and improve the reduction of the dispersed NiO species in catalyst, resulting in an improvement of the catalytic activity of Ce<sub>0.9-x</sub>Ni<sub>0.1</sub>Ca<sub>x</sub>O<sub>δ</sub>. The XRD and Raman results show that Ce<sub>0.9-x</sub>Ni<sub>0.1</sub>Ca<sub>x</sub>O<sub>δ</sub> (x ≤ 0.1) solid solution can form by Ni and Ca incorporation in the CeO<sub>2</sub> lattices. TEM and etching results reveal that part of Ni disperses well on the surface of Ca-doped sample. FT-IR testing shows that with an increase in Ca amount (x > 0.1), more carbonate species (mainly carbonate calcium) can form on the catalyst surface, which would severely debase the catalytic activity of Ce<sub>0.9-x</sub>Ni<sub>0.1</sub>Ca<sub>x</sub>O<sub>δ</sub>.

## Introduction

The catalytic combustion of methane has drawn a great attention in recent decades, because of the interests arising from environmental requirements and high burning efficiency [1, 2]. In general, the catalysts contain noble metals such as Pd and Pt are well known to be active for methane combustion at low temperature [3]. However, their commercialization is still limited by sintering and sublimation

at high temperature and the high cost of the noble metals [4]. Therefore, there is a strong demand for development of new, thermally stable, and low cost catalysts. Recent reports have shown that CeO<sub>2</sub>–NiO catalysts exhibit good catalytic activity for methane combustion [5, 6]. It has been reported that the addition of NiO to CeO<sub>2</sub> leads to an improvement in its redox properties and oxygen storage capacity by increasing the oxygen vacancy concentration and mobility of lattice oxygen, providing a new opportunity to develop efficient mixed oxide catalysts for the catalytic combustion of hydrocarbons [7, 8]. Yisup et al. [9] reported that the superior performance of the Ce–Ni–O mixed oxide catalysts could be attributed to the generation of highly dispersed NiO<sub>x</sub> species and the creation of highly active oxygen vacancies as a consequence of an easier incorporation of Ni<sup>2+</sup> ions into ceria lattice by the formation of solid solution in the mixed oxides. However, in order to satisfy the practical utilization, further study should be done to improve the thermal stability and the activity of the CeO<sub>2</sub>–NiO catalyst.

In the case of the ceria-based catalysts, increasing mobility of bulk oxygen by introducing defective sites can improve effectively the catalytic activity for the hydrocarbons oxidations [10]. It was reported that calcium-doped CeO<sub>2</sub> would tend to introduce defects and oxygen vacancies in the CeO<sub>2</sub> fluorite structure [11]. Moreover, our previous research study showed that the additives such as alkaline-earth in CeO<sub>2</sub>–ZrO<sub>2</sub> could improve the thermal stability [12]. The promotional effect of calcium on the thermal stability and catalytic property of Pd/Ce–Zr/Al<sub>2</sub>O<sub>3</sub> catalyst toward methane combustion was also obtained [13].

To the best of our knowledge, there is no report on exploring the effect of Ca doping on the CeO<sub>2</sub>–NiO composite oxide catalysts for methane combustion. In the present study, a series of Ce<sub>0.9-x</sub>Ni<sub>0.1</sub>Ca<sub>x</sub>O<sub>δ</sub> (x = 0–0.3)

D. Qiao · G. Lu (✉) · Y. Guo · Y. Guo  
Key Laboratory for Advanced Materials and Research  
Institute of Industrial Catalysis, East China University  
of Science and Technology, Shanghai 200237, China  
e-mail: gzlu@ecust.edu.cn

G. Lu · D. Mao  
Research Institute of Applied Catalysis, Shanghai  
Institute of Technology, Shanghai 200235, China

composite oxides were prepared by the citric acid complexation–combustion method, and characterized by the nitrogen adsorption–desorption, XRD, Raman, H<sub>2</sub>-TPR, and FT-IR techniques. The influence of Ca doping on the catalytic properties of CeO<sub>2</sub>–NiO composite oxides for methane combustion was investigated.

## Experimental

### Catalyst preparation

The Ce<sub>0.9-x</sub>Ni<sub>0.1</sub>Ca<sub>x</sub>O<sub>δ</sub> ( $x = 0\text{--}0.3$ ) catalysts were prepared by the citric acid complexation–combustion method [14, 15]. Ce(NO<sub>3</sub>)<sub>3</sub>·6H<sub>2</sub>O, Ni(NO<sub>3</sub>)<sub>2</sub>·3H<sub>2</sub>O, and Ca(NO<sub>3</sub>)<sub>2</sub>·2H<sub>2</sub>O salts were dissolved in de-ionized water with suitable ratios. Citric acid was added with 1.2 times of molar amounts to the premixed nitrate solutions of cerium, copper, and calcium. The obtained solution was stirred at 70 °C. Once the gel formed, temperature was elevated to 150 °C quickly, and the gel foamed vapors with production of nitrogen oxide and burned with sparks. A solid product was obtained after the sparks were extinguished. The as-obtained solid powder was calcined at 600 °C for 4 h in air and then grinded into 40–60 mesh, which referred to fresh sample. In order to compare their thermal stability, the catalysts were aged at 900 °C for 2 h.

### Catalyst characterization

Power X-ray diffraction patterns were recorded on a Rigaku D/max 2250VB/PC diffractometer with Cu K $\alpha$  radiation ( $\lambda = 1.5406 \text{ \AA}$ ) at scanning rate of 6°/min. The tube voltage and current were set at 40 kV and 100 mA, respectively. The N<sub>2</sub> adsorption–desorption isotherms were measured at 77 K on a NOVA 4200e Surface Area and Pore Size Analyzer. The samples were outgassed at 180 °C for 4 h before the measurement. The Brumauer–Emmett–Teller (BET) method was used to calculate the specific surface areas of samples, and the pore size distributions were obtained from the desorption data by the Barret–Joyner–Halenda (BJH) method, and the total pore volume was estimated at a relative pressure of 0.985. Transmission electron microscope (TEM) images were obtained on a JEOL JEM-1400 Transmission Electron Microscope. The Raman spectra were obtained on a Renishaw Raman spectrometer equipped with a CCD detector at ambient temperature and moisture-free conditions. The emission line at 514.5 nm from an Ar<sup>+</sup> ion laser (Spectra Physics) was focused, analyzing spot about 1 mm, on the sample under the microscope. The Fourier transform infrared (FT-IR) absorption spectra were recorded on a Nicolet NEXUS 670 FT-IR spectrometer, with 32 scans at an

effective resolution of 4 cm<sup>-1</sup>. The sample to be measured was ground with KBr and pressed into thin wafer for analysis. H<sub>2</sub>-temperature-programmed reduction (H<sub>2</sub>-TPR) of samples was carried out in a conventional flow system equipped with a thermal conductivity detector (TCD). 50 mg sample was loaded in the U-shaped quartz tube reactor. 5% H<sub>2</sub>/N<sub>2</sub> mixture gas of 45 mL/min was used, and a heating rate was 10 °C/min. H<sub>2</sub> consumption during the reduction was measured by TCD.

### Catalytic activity testing

The activities of Ce<sub>0.9-x</sub>Ni<sub>0.1</sub>Ca<sub>x</sub>O<sub>δ</sub> catalysts for methane combustion were tested in a quartz tube reactor at atmospheric pressure. The reagent gas consisted of 1.0% CH<sub>4</sub> + 4.0% O<sub>2</sub> in Ar was passed through the catalyst (100 mg) bed with a flow rate of 50 mL/min, and the space velocity (SV) was typically 30,000 mL/g h. The activity was monitored at 25–750 °C, with a heating rate of 5 °C/min. The reactants and products were analyzed online by gas chromatograph (GC) equipped with TCD. The catalysts activity was characterized by  $T_{50}$ ,  $T_{90}$  representing the reaction temperatures at methane conversion of 50% and 90%, respectively.

## Results and discussion

### XRD

Figure 1 shows the XRD patterns of the CeO<sub>2</sub> and Ce<sub>0.9-x</sub>Ni<sub>0.1</sub>Ca<sub>x</sub>O<sub>δ</sub> catalysts with different Ca contents. There are distinct diffraction peaks of CeO<sub>2</sub> in all the samples, which slightly shift towards low 2θ (the inset in Fig. 1). However, no diffraction peaks of NiO crystalline phase and Ca species can be observed. It was reported that the maximum solubility limit of Ca<sup>2+</sup> into CeO<sub>2</sub> is no more than 20 mol% [16]. Wrobel et al. [17] reported that Ni tends to insert in CeO<sub>2</sub> lattice to form a solid solution in low Ni content (Ni/Ce ≤ 0.5). It can be seen that the mean crystal size of ceria decreases with the increase of Ca content, based on the increase of the diffraction peak wide; the diffraction peak at 2θ = 59° turns weak gradually, and it disappears in the sample with  $x = 0.3$ . The results above show that Ni<sup>2+</sup> and Ca<sup>2+</sup> ions would simultaneously replace Ce<sup>4+</sup> in the CeO<sub>2</sub> fluorite structure to form the Ce<sub>0.9-x</sub>Ni<sub>0.1</sub>Ca<sub>x</sub>O<sub>δ</sub> solid solution in the low doping amount of Ni<sup>2+</sup> and Ca<sup>2+</sup>.

The lattice parameters, mean crystallize sizes (ceria cubic phase), and textural properties of the samples were listed in Table 1. It can be seen that a lattice parameter of Ce<sub>0.9</sub>Ni<sub>0.1</sub>O<sub>δ</sub> (0.5372 nm) decreases with Ni incorporated into CeO<sub>2</sub> (0.5399 nm), because the radius of Ni<sup>2+</sup>

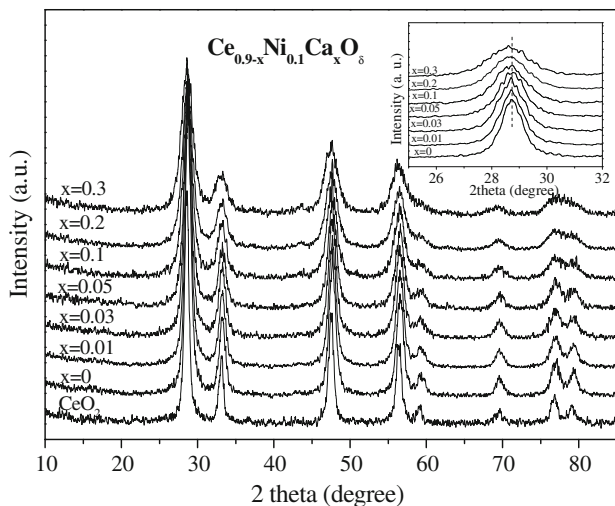


**Fig. 1** XRD patterns of fresh  $\text{CeO}_2$  and  $\text{Ce}_{0.9-x}\text{Ni}_{0.1}\text{Ca}_x\text{O}_6$  catalysts

( $0.69 \text{ \AA}$ ) is smaller than that of  $\text{Ce}^{4+}$  ( $0.97 \text{ \AA}$ ). Moreover, lattice parameter of  $\text{Ce}_{0.9}\text{Ni}_{0.1}\text{O}_6$  increases from  $0.5372 \text{ nm}$  with an increase in Ca amount in the sample, which confirms further that solid solution of  $\text{Ce}_{0.9-x}\text{Ni}_{0.1}\text{Ca}_x\text{O}_6$  has been formed by  $\text{Ca}^{2+}$  ions incorporating into the ceria lattice, because the radius of  $\text{Ca}^{2+}$  ( $1.12 \text{ \AA}$ ) is larger than that of  $\text{Ce}^{4+}$  ( $0.97 \text{ \AA}$ ) [18]. The aged samples present larger lattice constants compared with unaged ones, which could be attributed to the migration of Ni or Ca ions out of  $\text{CeO}_2$  lattice. The results in Table 1 show also that the BET surface areas of the Ca-doped samples ( $x \leq 0.05$ ) increase with addition of Ca; when  $x = 0.03$ , the maximum ( $35.5 \text{ m}^2/\text{g}$ ) can be obtained; the surface area decreases to  $16.0 \text{ m}^2/\text{g}$  with further increasing Ca amount. With an increase in the Ca amount in Ce–Ni–O, the pore volume decreases from  $0.093 \text{ cm}^3/\text{g}$  to  $0.046 \text{ cm}^3/\text{g}$ , and the average pore size increases from  $8.01 \text{ nm}$  to  $10.87 \text{ nm}$ . Moreover, the Ca doping in the sample results in a decrease of the crystal grain size of the ceria cubic phase from  $8.5 \text{ nm}$  to  $4.7 \text{ nm}$ .

**Table 1** BET surface areas, lattice constants, and average crystalline sizes and catalytic performances of the catalysts

Catalyst	BET surface area ( $\text{m}^2/\text{g}$ )	Pore volume ( $\text{cm}^3/\text{g}$ )	Average pore size (nm)	Lattice constant (nm) <sup>a</sup>	Crystal grain size (nm) <sup>b</sup>	$T_{50}$ (°C)	$T_{90}$ (°C)
$\text{CeO}_2$	18.1	0.051	12.15	0.5399	20.0	593	687
$\text{Ce}_{0.9}\text{Ni}_{0.1}\text{O}_6$	30.1	0.093	8.01	0.5372	8.5	503	617
$\text{Ce}_{0.87}\text{Ni}_{0.1}\text{Ca}_{0.01}\text{O}_6$	32.2	0.078	8.15	0.5376	8.2	484	572
$\text{Ce}_{0.87}\text{Ni}_{0.1}\text{Ca}_{0.03}\text{O}_6$	35.5	0.076	9.85	0.5383	8.0	466	557
$\text{Ce}_{0.85}\text{Ni}_{0.1}\text{Ca}_{0.05}\text{O}_6$	33.0	0.077	9.46	0.5388	7.4	488	578
$\text{Ce}_{0.8}\text{Ni}_{0.1}\text{Ca}_{0.1}\text{O}_6$	23.0	0.072	9.95	0.5395	6.2	499	603
$\text{Ce}_{0.7}\text{Ni}_{0.1}\text{Ca}_{0.2}\text{O}_6$	18.3	0.070	11.67	0.5400	5.1	588	670
$\text{Ce}_{0.6}\text{Ni}_{0.1}\text{Ca}_{0.3}\text{O}_6$	16.0	0.046	10.87	0.5400	4.7	613	695
$\text{Ce}_{0.9}\text{Ni}_{0.1}\text{O}_6^c$	3.6	—	—	0.5398	36.6	588	692
$\text{Ce}_{0.87}\text{Ni}_{0.1}\text{Ca}_{0.03}\text{O}_6^c$	4.7	—	—	0.5397	37.5	639	722

<sup>a</sup> Being calculated based on  $\text{CeO}_2$  (111) crystal plane; <sup>b</sup>the mean crystalline size of  $\text{CeO}_2$  fluorite was estimated from the Ce (111) line by the Scherrer formula; <sup>c</sup>being aged at  $900^\circ\text{C}$  for 2 h

Papavasiliou et al. [19] also reported that an addition of dopants (La, Mg, Y, or Ca) in  $\text{CuO}-\text{CeO}_2$  could cause a decrease in the surface area, which was not accompanied with a prospective increase in the  $\text{CeO}_2$  crystallite size.

## TEM

The TEM images of  $\text{Ce}_{0.9-x}\text{Ni}_{0.1}\text{Ca}_x\text{O}_6$  samples are shown in Fig. 2. As compared with the  $\text{CeO}_2-\text{NiO}$  sample, the image of the Ca-doped sample ( $x = 0.03$ ) shows that the NiO species disperse well in the sample (Fig. 2b) and have the average size of  $\sim 15 \text{ nm}$ , which also indicates that the Ca addition can promote the NiO species dispersion on the sample surface. Moreover, we used an etching method with nitric acid [20] to test the concentration of Ni on the surface, and the results show that the fraction of Ni located on the sample ( $x = 0.03$ ) surface is 22% of total Ni content in the sample. Therefore, part of Ni disperses on the surface of sample and its surface concentration is higher than that in the sample. In the image of the sample (Ca,  $x = 0.3$ ), there are many bright blocks, which may be aggregated carbonate species, and which can be validated by the FT-IR absorption spectra (Fig. 3).

## FT-IR spectroscopy

The FT-IR spectra of the prepared  $\text{Ce}_{0.9-x}\text{Ni}_{0.1}\text{Ca}_x\text{O}_6$  catalysts are presented in Fig. 3. The bands at  $1065$ ,  $1365$ , and  $1510 \text{ cm}^{-1}$  are observed in the sample with  $x = 0$ , which should be ascribed to unidentate carbonates [21]. It was reported that the carbonates can form favorably on the surface of solids containing  $\text{CeO}_2$ , due to the reconstruction surface or the surface basicity [22]. Therefore, it is deduced that these carbonate species probably in the form of cerium carbonates might be formed, due to adsorption of surrounding gas molecule. The bands at  $879$  and  $1450 \text{ cm}^{-1}$  should be assigned to carbonate calcium phase [23], which

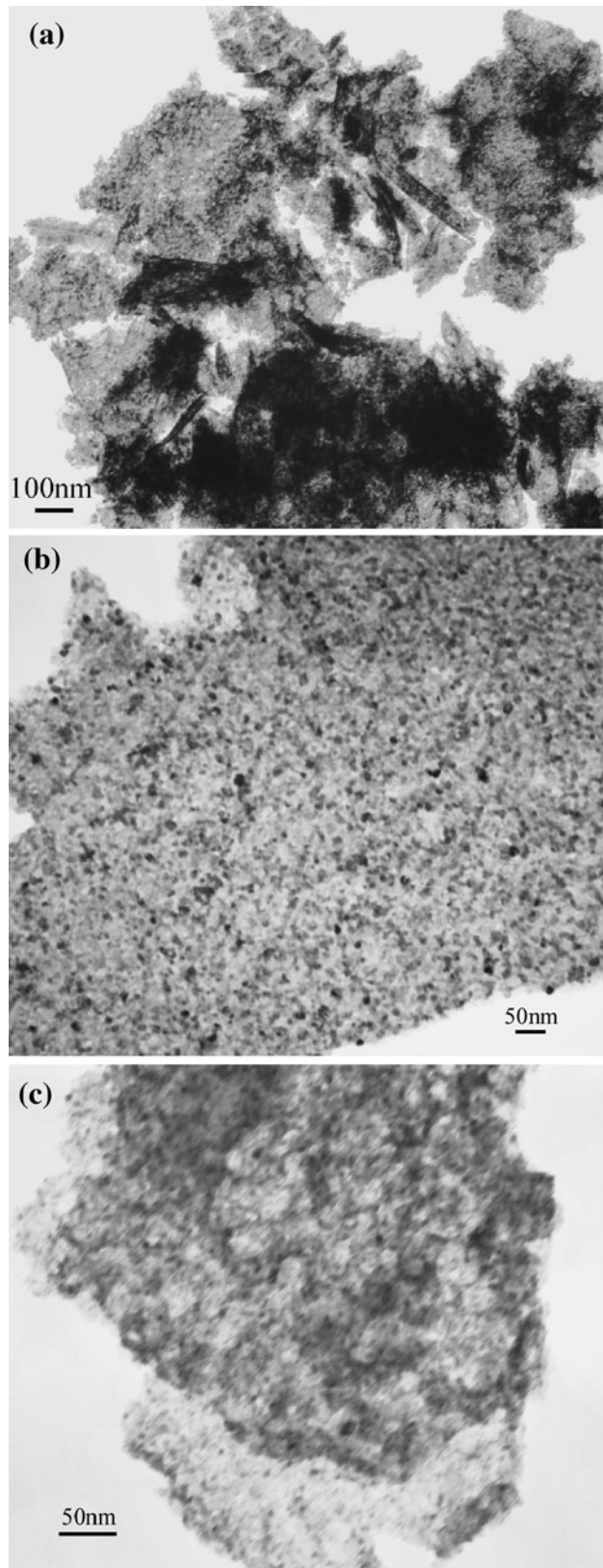


**Fig. 2** TEM images of  $\text{Ce}_{0.9-x}\text{Ni}_{0.1}\text{Ca}_x\text{O}_\delta$  of **a**  $x = 0$ , **b**  $x = 0.03$ , **c**  $x = 0.3$

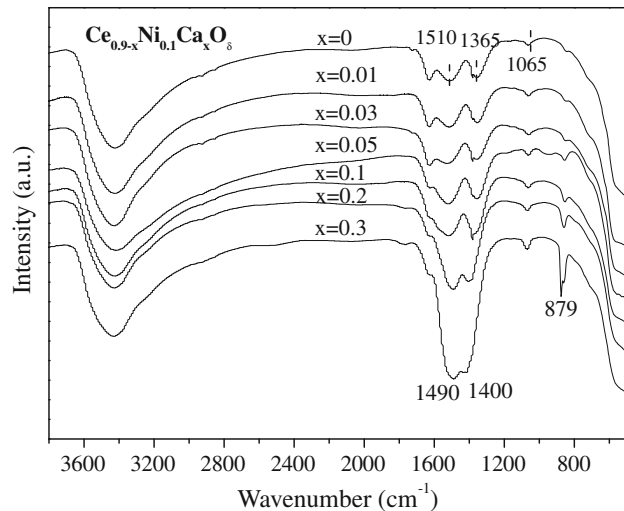


**Fig. 3** IR spectra of  $\text{Ce}_{0.9-x}\text{Ni}_{0.1}\text{Ca}_x\text{O}_\delta$  catalysts

are also observed in the TEM image in Fig. 2c. The intensities of these bands can be enhanced obviously with an increase in the Ca content ( $x \geq 0.05$ ). Based on the IR results, it can be found that more carbonate species (mainly carbonate calcium) would congregate on the surface of  $\text{Ce}_{0.9-x}\text{Ni}_{0.1}\text{Ca}_x\text{O}_\delta$  catalyst with an increase in the Ca content.

#### Raman spectroscopy

Figure 4 shows the Raman spectra recorded using a laser at 514.5 nm as the excitation source, and a broad band with relatively high intensity at  $\sim 461 \text{ cm}^{-1}$  and a weak band at  $1172 \text{ cm}^{-1}$  were observed, which are ascribed to the  $F_{2g}$  vibration mode and primary  $A_{1g}$  asymmetry of  $\text{CeO}_2$ , respectively [24]. The bands at 557 and  $633 \text{ cm}^{-1}$  in the sample with  $x < 0.05$  should be ascribed to NiO species [25], which suggested that highly dispersed NiO exists on the surface of the samples, which was also observed in the TEM results in Fig. 2b. Pati et al. [20] also reported that the surface enrichment or segregation of transition metal oxides ( $\text{CuO}$ ,  $\text{NiO}$ , and  $\text{Fe}_2\text{O}_3$ ) on ceria was detected by X-ray photoelectron spectroscopy. The band at  $\sim 590 \text{ cm}^{-1}$  is linked to lattice defects resulted from the produced oxygen vacancies in the ceria fluorite structure [26]. With an increase in Ca amount, the Raman peaks of  $\text{CeO}_2$  shift to lower wave number region as shown in the enlarged graphic (the inset in Fig. 4). This phenomenon could be attributed to the formation of  $\text{Ce}_{0.9-x}\text{Ni}_{0.1}\text{Ca}_x\text{O}_\delta$  solid solution with Ni and Ca ions replacing Ce ions in  $\text{CeO}_2$  lattice. The appearance of well-defined bands at 225 and  $590 \text{ cm}^{-1}$  confirms the solid solution formation [9]. With further increase of Ca amount, the intensities of bands at

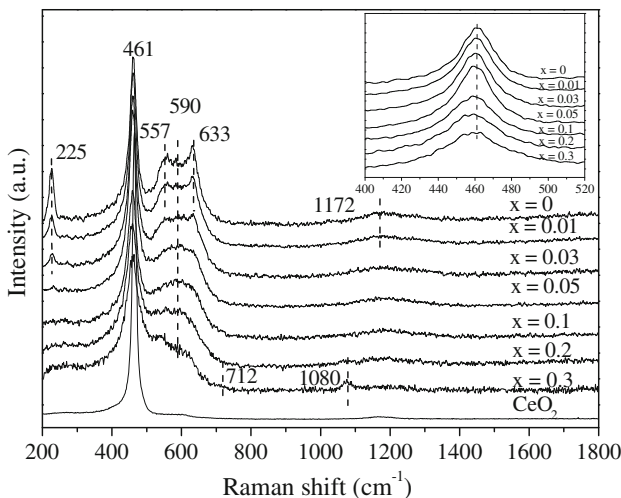


**Fig. 4** Raman spectra of  $\text{CeO}_2$  and  $\text{Ce}_{0.9-x}\text{Ni}_{0.1}\text{Ca}_x\text{O}_\delta$  catalysts

225, 460, and  $590 \text{ cm}^{-1}$  decreases accordingly, suggesting that the presence of Ca with high amount might change the M–O bonding symmetry or the samples were covered by the increasing amount of carbonate species shown in Fig. 2c. The weak bands at 712 and  $1080 \text{ cm}^{-1}$  are observed in the samples with  $x \geq 0.2$ , which should be assigned to the carbonate species [27].

#### H<sub>2</sub>-TPR

The TPR profiles of  $\text{Ce}_{0.9-x}\text{Ni}_{0.1}\text{Ca}_x\text{O}_\delta$  samples are shown in Fig. 5. At  $<600 \text{ }^\circ\text{C}$ , there are three H<sub>2</sub> consumption peaks ( $\alpha_1$ ,  $\alpha_2$ , and  $\beta$ ) for the sample with low Ca content ( $x < 0.1$ ). The  $\alpha_1$  and  $\alpha_2$  peaks should be ascribed to the reduction of adsorbed oxygen on the surface of solid solution; the  $\beta$  peak is attributed to the reduction of highly dispersed NiO on the surface of  $\text{CeO}_2$ . The  $\alpha$  and  $\beta$  peaks

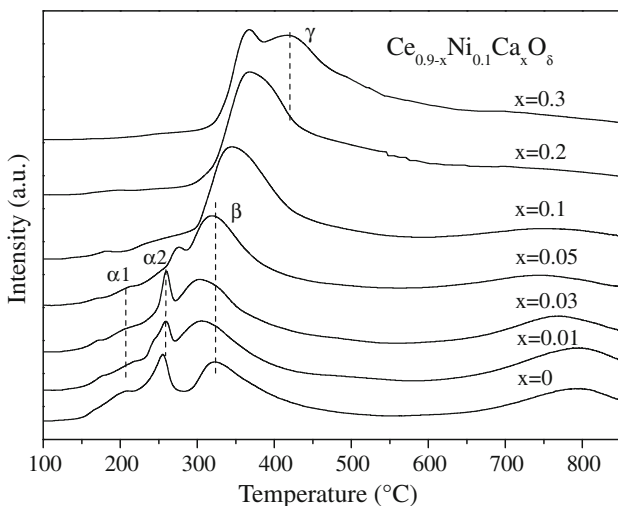


**Fig. 5** H<sub>2</sub>-TPR profiles of  $\text{Ce}_{0.9-x}\text{Ni}_{0.1}\text{Ca}_x\text{O}_\delta$  catalysts

provide the main active sites of methane catalytic combustion [5]. Comparing with Ca-undoped sample, the  $\beta$ -reduction peaks shift to lower temperature for the sample with  $x < 0.1$ , which is due to the formation of solid solution and higher surface areas of the samples induced by Ca doping. When Ca content is higher ( $x > 0.1$ ), the  $\beta$ -reduction peaks shift to higher temperature, which should be attributed to the congregated carbonate species on the sample surface, which makes the reduction of NiO species difficult. The  $\gamma$ -reduction peak at  $\sim 420 \text{ }^\circ\text{C}$  in the sample with  $x = 0.3$  should be ascribed to the reduction of aggregated NiO particles [19]. The weak reduction peak at about  $800 \text{ }^\circ\text{C}$  should be attributed to the reduction of bulk oxygen of crystalline  $\text{CeO}_2$  [28]. With an increase in Ca content, this peak at  $\sim 800 \text{ }^\circ\text{C}$  shifts toward lower temperature and varies gradually until this peak becomes inconspicuous.

#### Catalytic activity for methane combustion

Figure 6 shows the catalytic performances of  $\text{Ce}_{0.9-x}\text{Ni}_{0.1}\text{Ca}_x\text{O}_\delta$  catalysts for the methane combustion, and the catalytic activities in terms of  $T_{50}$ ,  $T_{90}$  are listed in Table 1. During methane combustion reaction, CH<sub>4</sub> was completely oxidized to CO<sub>2</sub> and H<sub>2</sub>O. For the catalysts with  $x \leq 0.1$ , the addition of Ca can promote the activities of the catalysts, and the catalyst with  $x = 0.03$  behaves superior performance, such as  $T_{50} = 466 \text{ }^\circ\text{C}$  and  $T_{90} = 557 \text{ }^\circ\text{C}$ . The presence of the easier reduction NiO species and the increased surface area, which are induced by the Ca doping help in promoting the catalytic activity of the catalysts. When  $x > 0.1$  in the catalyst, the presence of Ca makes its activity decrease obviously, and it is possible that the active sites of the catalyst are covered partly by the congregated carbonates species as shown in Fig. 3. It is well known, the high mobility of surface and bulk oxygen of ceria-based catalysts by introducing defective sites, can effectively promote the hydrocarbons oxidation reactions [29, 30]. Therefore, the oxygen vacancies formed by doping Ca in  $\text{CeO}_2$ –NiO should be benefit to methane catalytic combustion. It was reported that the basicity of the catalyst is important to activate the C–H bond, due to the very weakly acidic C–H bond in methane ( $pK_a = 46$ ) [31]. In the  $\text{CeO}_2$ –NiO sample, the addition of Ca can improve its basicity, which was validated by the FT-IR results, and help to activate the C–H bond of methane, resulting in improvement of its catalytic activity for the methane combustion.

To evaluate the effect of Ca doping on thermal stabilities of  $\text{Ce}_{0.9-x}\text{Ni}_{0.1}\text{Ca}_x\text{O}_\delta$  catalysts, the catalysts ( $x = 0$  and 0.03) were aged in air at  $900 \text{ }^\circ\text{C}$  for 2 h, and the light-off curves for methane combustion over these aged catalysts are shown in Fig. 7. The results show that the catalytic

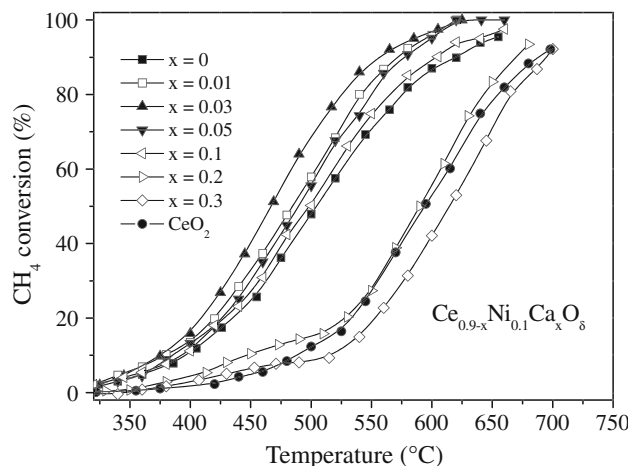


**Fig. 6** Light-off curves for methane catalytic combustion over  $\text{CeO}_2$  and  $\text{Ce}_{0.9-x}\text{Ni}_{0.1}\text{Ca}_x\text{O}_\delta$  catalysts

performance of the catalyst ( $x = 0$  or  $0.03$ ) decrease obviously after being aged, which should account for the larger average crystalline size and lower surface area of the aged catalysts (Table 1), comparing with unaged or fresh catalysts. For the unaged catalyst, the Ca-doped catalyst behaves higher performance than the Ca-undoped catalyst; after being aged the inverse result is obtained, that is, over the Ca-doped catalyst  $T_{50} = 639^\circ\text{C}$ , and over the Ca-undoped catalyst  $T_{50} = 588^\circ\text{C}$ .

In order to explain the reason for a low activity of the aged sample, the  $\text{H}_2$ -TPR was used to test the surface reduction of the aged samples, and the results are shown in Fig. 8. It can be seen that the intensities of  $\alpha 1$  and  $\alpha 2$  peaks are very weak (the sample of  $x = 0$ ) or disappeared ( $x = 0.03$ ) after the sample is aged, which should account for the very low amount of surface oxygen and be partly due to the low surface areas of the aged samples. Compared with the fresh

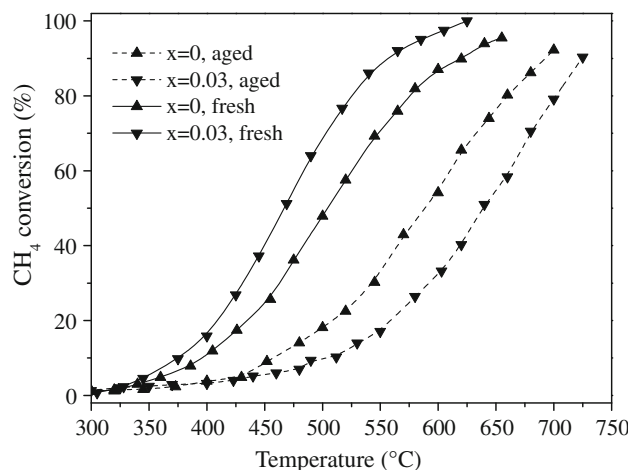


**Fig. 7** Light-off curves for methane catalytic combustion over fresh and aged ( $900^\circ\text{C}/2\text{ h}$ )  $\text{Ce}_{0.9-x}\text{Ni}_{0.1}\text{Ca}_x\text{O}_\delta$  catalysts

samples, the intensities of  $\beta$ -reduction peaks get stronger and shift to higher temperature of  $338^\circ\text{C}$  (the sample of  $x = 0$ ) and  $380^\circ\text{C}$  ( $x = 0.03$ ), which indicates that  $\text{NiO}$  dispersed in  $\text{CeO}_2$  could be sintered and aggregate to larger  $\text{NiO}$  particles after being aged. The fact that the increased lattice parameters of the aged samples ( $\text{CeNiO}$ ,  $0.5398\text{ nm}$ ;  $\text{CeNiCaO}$ ,  $0.5397\text{ nm}$ ) are close to the pure  $\text{CeO}_2$  ( $0.5399\text{ nm}$ ), implies that Ni or Ca in solid solution could migrate out of  $\text{CeO}_2$  lattice to form  $\text{NiO}$  particles or Ca species. Therefore, the increased amount of  $\text{NiO}$  particles on  $\text{CeO}_2$  should contribute to an augmentation of  $\beta$  peak area of the aged samples. For the aged Ca-doped sample, the Ca-including species might be formed on the surface of  $\text{CeO}_2$  by migration of Ca ions out of bulk  $\text{CeO}_2$ , and debase the reduction of  $\text{NiO}$  species. This should be the main reason for the low activity of the aged Ca-doped catalysts.

The results show that Ca doping could not improve the thermal stability of the  $\text{Ce}_{0.9}\text{Ni}_{0.1}\text{O}_\delta$  solid solution catalysts, and we should develop the novel preparation method to improve the thermal stability of the Ca-doped  $\text{Ce}_{0.9}\text{Ni}_{0.1}\text{O}_\delta$  catalyst.

## Conclusions

The  $\text{Ce}_{0.9-x}\text{Ni}_{0.1}\text{Ca}_x\text{O}_\delta$  solid solutions can be obtained by a citric acid complexation–combustion method, in which Ca and Ni ions doped into the ceria lattices. The doping of Ca can affect the specific surface area and the mean crystalline size of the sample. As  $x \leq 0.1$ , the presence of Ca can enhance the catalytic performance of  $\text{Ce}_{0.9-x}\text{Ni}_{0.1}\text{Ca}_x\text{O}_\delta$  for methane combustion, due to larger surface area and the easier reduction of the dispersed  $\text{NiO}$  species. With the

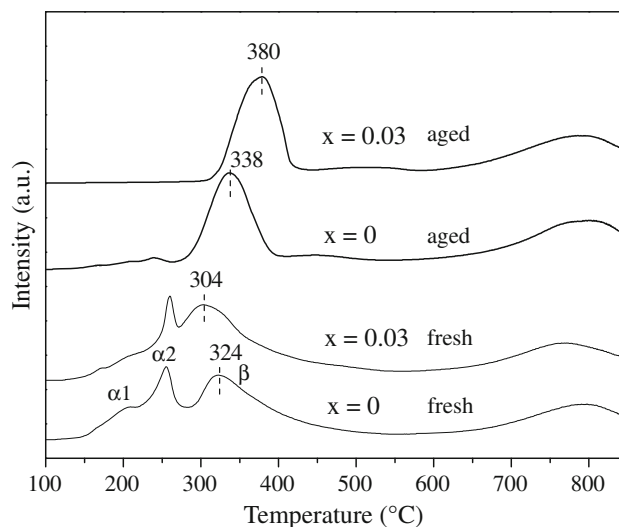


**Fig. 8**  $\text{H}_2$ -TPR profiles of the fresh and aged  $\text{Ce}_{0.9-x}\text{Ni}_{0.1}\text{Ca}_x\text{O}_\delta$  ( $x = 0, 0.03$ ) catalysts

increase of Ca content ( $x > 0.1$ ) in the samples, more carbonate species would be formed on the surface of catalyst, which would debase the catalytic performance. Moreover, the Ca doping could not improve the thermal resistance of the catalyst.

**Acknowledgements** We would like to acknowledge the financial support from National Basic Research Program of China (2010CB732300) and the Education Committee of Shanghai (J51503).

## References

1. Forzatti P, Groppi G (1999) *Catal Today* 54:165
2. Lampert JK, Shahjahan Kazi M, Farrauto RJ (1997) *Appl Catal B Environ* 14:211
3. Choudhary TV, Banerjee S, Choudhary VR (2002) *Appl Catal A Gen* 234:1
4. Farrato RJ, Hobson MC, Kennelly T, Waterman EM (1992) *Appl Catal A Gen* 81:227
5. Shan WJ, Luo MF, Ying PL, Shen WJ, Li C (2003) *Appl Catal A Gen* 246:1
6. Li Y, Guo Y, Xue B (2009) *Fuel Process Techol* 90:652
7. Jalowiecki-Duhamel L, Ponchel A, Lamonié C, Huysser AD, Barbaux Y (2001) *Langmuir* 17:1511
8. Potdar HS, Roh HS, Jun KW, Ji M, Liu ZW (2002) *Catal Lett* 84:95
9. Yisup N, Cao Y, Feng W, Dai W, Fan K (2005) *Catal Lett* 99:207
10. Terribile D, Trovarelli A, Leitenburg C, Primavera A, Dolcetti G (1999) *Catal Today* 47:133
11. Rodriguez JA, Wang XQ, Hanson JC, Liu G (2003) *J Chem Phys* 119:5659
12. Wang XH, Lu GZ, Guo Y, Jiang LZ, Guo YL, Li CZ (2009) *J Mater Sci* 44:1294. doi:[10.1007/s10853-009-3275-4](https://doi.org/10.1007/s10853-009-3275-4)
13. Yue BH, Zhou RR, Zheng XM, Lu WC (2008) *Fuel Process Technol* 89:728
14. Taguchi H, Matsuoka S, Kato M, Hirota K (2009) *J Mater Sci* 44:5732. doi:[10.1007/s10853-009-3802-3](https://doi.org/10.1007/s10853-009-3802-3)
15. Li YY, Yao SS, Xue LH, Yan YW (2009) *J Mater Sci* 44:4455. doi:[10.1007/s10853-009-3673-7](https://doi.org/10.1007/s10853-009-3673-7)
16. Yan M, Mori T, Ye F, Ou DR, Zou J, Drenna J (2008) *J Eur Ceram Soc* 28:2709
17. Wrobel G, Sohier MP, Huysser AD, Bonnelle JP (1993) *Appl Catal A Gen* 101:73
18. Yamashita M, Kameyama K, Yabe S, Yoshida S, Fujishiro Y, Kawai T, Sato T (2002) *J Mater Sci* 37:683. doi:[10.1023/A:1013819310041](https://doi.org/10.1023/A:1013819310041)
19. Papavasiliou J, Avgouropoulos G, Ioannides T (2007) *Appl Catal B Environ* 69:226
20. Pati RK, Lee IC, Hou S, Akhuemonkhan O, Gaskell KJ, Wang Q, Frenkel AI, Chu D, Salamanca-Riba LG, Ehrman SH (2009) *ACS Appl Mater Interface* 1:2624
21. Li C, Arai T, Domen K, Maruya K, Onishi T (1989) *J Chem Soc Faraday Trans* 85:929
22. Djinović P, Levec J, Pintar A (2008) *Catal Today* 138:222
23. Mikkelsen A, Engelsen SB, Hansen HCB, Larsen O, Skibsted LH (1997) *J Cryst Growth* 177:125
24. Weber WH, Hass KC, McBride JR (1993) *Phys Rev B* 48:178
25. Chan SS, Wachs IE (1987) *J Catal* 103:224
26. Martinez-Arias A, Gamarra D, Fernandez-Garcia M, Wang X, Hanson J, Rodriguez J (2006) *J Catal* 240:1
27. Devarajan A, Abdul Khadar M, Chattopadhyay k (2007) *Mater Sci Eng A* 452–453:395
28. Ricote S, Jacobs G, Milling M, Ji Y, Patterson PM, Davis BH (2006) *Appl Catal A Gen* 303:35
29. Godinho M, Goncalves RD, Leite ER, Raubach CW, Carreno NLV, Probst LFD, Longo E, Fajardo HV (2010) *J Mater Sci* 45:593. doi:[10.1007/s10853-009-3932-7](https://doi.org/10.1007/s10853-009-3932-7)
30. Wolf D (1994) *Catal Lett* 27:207
31. Burch R, Crittle DJ, Hayes MJ (1999) *Catal Today* 47:229